Biointerface Research in Applied Chemistry
Open-Access Journal (ISSN: 2069-5837)

Article
Volume 15, Issue 5, 2025, 69
https://doi.org/10.33263/BRIAC155.069

Microbial-Induced Corrosion on Copper Coupons and Resistance of Corrosion by Copper Nanoparticles

Johann Abraham [1,2], Mrunal Shetty [1], Anushree Suresh [3], Jeevanantham A K [1], Jayanthi Abraham [2,*]

[1] Department of manufacturing engineering, School of mechanical engineering, VIT, Vellore - 632014, Tamil Nadu, India
[2] Data analytics, School of Management, Binghamton University, SUNY, New York, USA
[3] Microbial Biotechnology Laboratory, School of Bio-Sciences and Technology, VIT, Vellore-632014, Tamil Nadu, India
* Correspondence: jayanthi.abraham@gmail.com; jayanthi.abraham@vit.ac.in;

Received: 5.05.2025; Accepted: 24.07.2025; Published: 10.08.2025

Abstract: The research project discusses the anti-corrosion behaviour of copper chloride nanoparticles synthesized. The corrosion behaviour mechanism of the copper coupon was investigated using bacterial and fungal isolates. Surface or topological analysis was performed using SEM and AFM analytical methods. The weight loss results revealed that a higher corrosion rate was observed in bacterial-treated (0.40 ± 0.1 mm/y) compared with that of fungal-treated (0.26 ± 0.01 mm/y) at the end of the exposure period of 336 h. Microbial colonies accelerate corrosion by creating localized corrosive environments. The corrosion rate of copper exposed to bacteria was found to be 0.033 mm/year, and that of fungi was found to be 0.016 mm/year. Scanning electron microscopic images of both nanoparticles-coated copper coupons and the epoxy nanoparticle-coated workpiece exhibited no pitting and a smooth surface, thereby showing anti-corrosive properties.

Keywords: AFM; anticorrosion; biocorrosion; copper coupons; surface topology; nanoparticles; surface response

1. Introduction

Microbial-mediated corrosion or biocorrosion has been referred to as one of the major problems on the global scale, affecting many important industries and municipal services such as oil refineries, shipping, construction, water treatment plants, nuclear power generation, etc., to name a few [1]. Acids and other corrosive chemicals are known to play the role of a catalyst to stimulate the anodic reaction[2]. Furthermore, on the consumption of these ions, microorganisms catalyse the cathodic reactions, thereby secreting secondary metabolites such as enzymes and acids that aid in biocorrosion [3]. Over the years, it has become clear that microbes not only cause corrosion but also act as inhibitors against anti-corrosive agents [4].

Sulfate-reducing bacteria (SRB), iron-reducing bacteria, iron-oxidizing bacteria, acid-producing bacteria, and fungi are all known to have MIC on metals [5]. MIC has been difficult to combat due to its capability to act independently and also to coexist with other corrosion mechanisms [6]. Copper and its alloys are commonly employed in a wide range of applications, including household and industrial piping, heat exchangers, fire protection systems, and marine structures due to their excellent workability, superior thermal and electrical conductivity, easy

solderability, and remarkable corrosion resistance. This corrosion resistance is largely attributed to the development of a protective patina on the surface, which promotes passivation when exposed to oxygen. [6,7]. The recycled water content of recirculation water is greater than that of fresh water. This encourages the growth of biofilms and corrosion [8].

Extracellular polymeric substances (EPSs) aid microbial cell adherence to iron surfaces and the formation of biofilms on metal surfaces. EPSs are thought to be polymeric conglomerations (proteins, polysaccharides, and lipids) that allow iron ions to be bioabsorbed [9]. In general, EPSs are made up of functional groups that may easily bond to metal surfaces, enhancing corrosion rates caused by biofilms and improving cathodic reactions [10]. Due to their good insulating capabilities, ease of manufacture, and low cost, mild steel (MS) and brass (BR) are being utilised widely as metals in CWSs [11].

Corrosion inhibition can be achieved by coating the material surface with passive films or active conversion coatings. To avoid oxidation, they provide low-density holes or stimulate surface biochemical processes. Metallic nanoparticles have piqued researchers' interest in this field due to their intriguing optical, electrical, and catalytic capabilities [12]. Copper is a naturally occurring element and an important micronutrient for all aerobic living forms [13]. It is thought to be important in the development and maintenance of the neurological and cardiovascular systems, as well as the muscular, immunological, and reproductive systems in humans [14]. In many situations, copper can limit the growth of microorganisms, giving some protection against hazardous germs and bacteria. There have been a number of techniques developed for the manufacture of copper nanostructures, including chemical reduction, sono-chemical reduction, metal vapour synthesis, and microemulsion [15]. Most copper nanoparticles are made by chemical sol-gel methods because they are simple, low-cost, and easy to control in terms of size and shape.

The current study investigates the anti-corrosion activity of copper chloride nanoparticles against the copper workpiece and the corrosion study using bacterial and fungal isolates for exposure periods of 6 h, 24h, 48 h, 168 h, and 336 h.

Materials and Methods

2.1. Chemicals.

Chemicals and all reagents (≥ 99% purity) were obtained from HiMedia Labs, Mumbai, India, and Sisco Research Laboratories Pvt. Ltd., Mumbai. In all cases, the reagents used were 99.9% pure and purchased from SRL chemicals.

2.2. Sample collection.

Soil sample was collected from the sewage area near VIT (latitude - 12.9721◦N, longitude -79.1596◦E), Vellore, Tamil Nadu, India. An air-dried sample of soil was collected and stored at room temperature. It is sieved to remove gravel and stored carefully for laboratory analysis.

2.3. Enrichment and isolation of microorganisms from the collected samples.

2.3.1. Enrichment of bacteria.

The enrichment technique was performed by adding 10g of the soil sample in 100 ml of MSM media comprising Potassium Phosphate Monobasic (KH_2PO_4)-1g, Sodium Nitrate

($NaNO_3$)-1.5 g, Magnesium Sulphate ($MgSO_4.7H_2O$)-0.5 g, Ferrous sulphate ($FeSO_4$-0.01 g), Ammonium Sulphate $(NH4)_2SO_4$-1.5 g, Calcium chloride ($CaCl_2$)-0.002 g in 250 ml Erlenmeyer flask which was supplemented with 1mg/ml concentration of Cu_2SO_4. Flask was placed in a rotary shaker at 180 rpm for 3-4 days at 30°C [16].

2.3.2. Enrichment of fungi.

The enrichment technique for fungi was performed by adding 10 g of the soil sample in 100 ml of M1 media comprising sodium nitrate ($NaNO_3$)-2 g, Potassium chloride (KCl) – 0.5 g, Magnesium sulphate ($MgSO_4.7H_2O$) -0.5 g, glucose- 10 g, Ferric chloride ($FeCl_3$)-0.1 g, Barium chloride ($BaCl_2$)-0.2 g, Calcium chloride ($CaCl_2$)-0.5 g in 250 ml Erlenmeyer flask which was supplemented with 1mg/ml concentration of Cu_2SO_4. The flask was incubated in a rotary shaker at 180 rpm for 5 days at 28°C [16].

2.4. Isolation and maintenance of microorganisms for further analysis.

Serial dilutions (10^{-1} to 10^{-5}) were prepared from the enriched soil suspensions using sterile test tubes. For bacterial isolation, 1 mL of MSM containing 1 mg/mL $CuSO_4$ was used as the diluent, and 100 µL aliquots from the 10^{-5} to 10^{-7} dilutions were spread onto MSM agar plates. For fungal isolation, 1 mL of M1 medium supplemented with 1 mg/mL $CuSO_4$ was used, and 100 µL from the 10^{-2} to 10^{-4} dilutions were plated onto M1 agar. All plates, including controls, were incubated at 37 °C for bacterial plates for 48 h and fungal plates for 5–6 d. Colonies were selected based on distinct morphology for further analysis [17].

2.5. Identification of the isolated strains.

2.5.1. Gram staining and biochemical tests.

Gram staining was performed to identify the Gram nature of the bacterial isolate. (1) Gram staining, (2) starch content, (3) indole production, (4) citrate utilisation test, (5) methyl red test, (6) Voges-Proskauer test, (7) catalase test, (8) carbohydrate fermentation test, (9) gelatin content, (10) oxidase test, (11) motility test, and (12) lipid hydrolysis test were used to identify the resulting bacterial isolate.

2.5.2. Lactophenol cotton blue staining (LPCB).

Lactophenol cotton blue (LPCB) wet mount preparation is the most familiar primary method of staining. A wet mount was prepared by adding a drop of lactophenol cotton blue stain on a clean, grease-free, and dry glass slide. The fungal culture was smeared on the stain and tweezed carefully to separate the different structures of the organism. The slide was then viewed under 40x and 100x (oil immersion) for clear morphological observation.

2.5.3. Molecular characterization.

A potent bacterial and fungal isolate was used to extract genomic DNA. PCR amplification of the isolates' 16s rRNA (bacterial) and 28s rRNA (fungal) genes was performed using 1.5 µL of forward and reverse primers, 5 µL of deionized water, and 12 L of Taq Master Mix (Taq DNA polymerase provided in 2X Taq buffer, 0.4 mM dNTPs, 3.2mM $MgCl_2$, and 0.02% bromophenol blue). Following the amplification, the DNA was denaturised for 5 mins at 94°C, annealed for 30 secs at 51°C, and then extended at 72°C with $MgCl_2$ at a final

concentration of 1.5 mM. The PCR results were sequenced using the primers. The sequencing processes were carried out using ABI PRISM® BigDyeTM Terminator Cycle Sequencing Kits with AmpliTaq® DNA polymerase (FS enzyme) (Applied Biosystems). The phylogenetic position of the potent fungal strain was determined using a nucleotide sequence database search using the BLAST tool from the National Center for Biotechnology Information (NCBI) GenBank. The GenBank NCBI received the findings of the nucleotide sequencing, and an accession number was given. A new neighbour was added to the phylogenetic tree using the Mega 5.0 programme [16].

2.6. Experimental set-up.

2.6.1. Mechanical preparation of copper coupons.

Cu workpieces were cut using Wire Electric Discharge Machining. WEDM is an electro-thermal machining process for electrically conductive materials. Each metal coupon was ground using a series of grit silicon carbide sheets (grades 180, 500, 800, 1200, and 1500) to generate a flat metal surface, and then polished with micron alumina (0.3) powder to a mirror sheen. The refined coupons were washed with distilled water before being immersed in a 70% ethanol solution for 1 min to sterilise the surface thoroughly. The coupons were sterilised and then kept in a desiccator. For the weight reduction experiment, the metal coupon employed in the current study was 1.0 cm x 1.0 cm x 0.3 cm in size [18].

2.6.2. Microbial-mediated corrosion.

The bacterial suspension of freshly prepared 1.00 O.D. was inoculated into MSM media. Similarly, the fungal spore suspension of freshly prepared was inoculated into M1 media in 250 ml Erlenmeyer flask. Using a fed-batch culture method, a 336h continuous corrosion system was set up for analysis. Each sector had 4 copper workpieces that were immersed in different 250 mL Erlenmeyer flasks containing 100 mL culture medium. A total of five trials were conducted for each metal corrosion study. Flasks without bacterial and fungal suspension were maintained as controls. The flasks were incubated on a rotary shaker (Lark shaker incubator) at 37°C at 121 rpm for 336 h; meanwhile, copper samples were collected after 6h, 24 h, 48 h, 168 h, and 336 h of immersion. Each condition was tested in triplicate. The corrosion was studied after analyzing the assets of metal coupons in a post-corrosion study. The microbiologically induced corrosion was analyzed using SEM-EDAX [19].

2.6.3. Topographical surface analysis of workpiece using analytical techniques.

The metal coupons were washed with sodium dodecyl sulfate solution and then dried using an air drier for the weight loss experiment. Each system was tested in triplicate. The final weights of each coupon were obtained every 6 h, 24 h, 48 h, 168 h, and 336 h. The average corrosion rates were then calculated using the NACE standard method (NACE 2005). After the corrosion experiment, the corrosion products were carefully gathered and put through a surface inspection (XRD, AFM, and SEM) [20]. The corrosion products were ground into a fine powder and analysed using XRD. The temperature range of the system-controlled XRD (Bruker-8030) was 2 to 85 degrees. SEM (Ultra55 model, Zeiss, Germany) investigations were conducted to examine the bacterial clustering. The specimen was coated with gold-palladium to obtain the scanned secondary electron picture [21]. To more accurately assess the underlying

corrosion damage to the metal, typical corrosion pits were selected for measurement. The elemental makeup of corrosion products was examined using energy-dispersive spectroscopy (EDS, Oxford IE450X-Max80 model, Zeiss, Germany). The concordant results were determined to be highly reproducible after three sets of all measurements were made. The samples' precise size, shape, and aggregation at the maximum time point of nanoparticle formation were examined using atomic force microscopy (model: Nanosurf EasyScan 2 AFM, made in Switzerland). AFM chromatograms were captured using silicon cantilevers with force constants ranging from 0.02 to 0.07 N/m and a tip height of 10–15 nm in contact mode. The coupons were taken out of the inoculation media after the prescribed exposure time, rinsed twice in sterile deionized water to eliminate any remaining dead or loosely attached microorganisms, dried by purging with nitrogen, and then stored in an airtight vacuum desiccator for inspection in air by AFM. The following is the mathematical formula developed by Fontana to determine the rates of sample corrosion following weight loss measurement:

$$CR = 87.6W\rho AT\ (\frac{\text{mm}}{\text{year}}) \qquad (1)$$

Where CR = corrosion rate in mm per year, w = weight loss in mg, this was done by subtracting the final weight measured from the initial weight which gave the weight loss (weight difference), ρ = density of each sample in mg/m^3, A = area, the area of each sample was determined by calculating the total surface area in cm^2 and T = time, this was an exposure time in h of each of the samples spent inside the different concentrations of the acidic media [22].

2.7. Minimum inhibitory concentration of copper chloride nanoparticle.

Well diffusion assay was used to detect the minimum inhibitory concentration of nanoparticles on copper metal effective against isolates. Various concentrations of nanoparticles- 0.1 mg/ml, 0.25 mg/ml, 0.5 mg/ml, and 1.0 mg/ml were used for this study. Freshly prepared two bacterial culture suspensions of 1 O.D. were swabbed onto each Muller-Hinton agar plate. Six wells were bored using a sterile well borer, and 100 µl of different concentrations of nanoparticles were added. Distilled water served as the negative control, and amoxicillin (1 mg/ml) served as the positive control. The plates were incubated for 24 h at 37°C. The zones of inhibition were recorded [23].

2.8. Synthesis of copper chloride nanoparticles using the sol-gel method.

Copper (II) chloride nanoparticles were synthesized via a sol-gel method. A 0.01 M $CuCl_2$ $2H_2O$ solution was prepared in 500 mL of deionized water, and a 1.0 M L-ascorbic acid solution was added as the reducing agent. The mixture was heated in a water bath shaker at 90°C for 3 h under continuous stirring. The pH of the solution was adjusted to ~6.5 using dilute NaOH. A gradual colour change from pale blue to dark brown indicated nanoparticle formation. The resulting product was centrifuged, washed with ethanol and deionized water, and dried at 60°C for 24 h. The final yield was approximately 82% (w/w) based on initial copper salt weight [24].

2.9. Effect of nanoparticles on biocorrosion of workpiece.

2.9.1. Anti-corrosion nature of copper chloride nanoparticle.

For 336 h on a rotary shaker (Lark shaker incubator) at 37°C at 121 rpm, copper chloride nanoparticle at a concentration of 1 mg/ml was applied to MSM broth flasks with bacterial isolates and M1 media with fungi isolates, respectively, with 4 copper workpieces. Surface topology was analysed using analytical techniques such as SEM and AFM. Copper chloride nanoparticles were not coated onto the copper workpiece but added into the MSM broth media along with the microbes.

2.10. Growth kinetics of potent bacteria and fungi.

The growth behaviours of the bacterial strain were examined in mineral salt medium (MSM) broth. In MSM broth, the strain was isolated and cultivated for 24 h. The bacterial culture's broth was diluted to a 10^{-1} concentration after incubation and used to inoculate the medium to track growth over time. A change in the growth trend was discovered by estimating the optical density at 600 nm [25]. The growth patterns of the fungi were determined by checking the dry weight of the fungal biomass at regular intervals. The fungal strains were inoculated individually in minimal (M1) broth and incubated at 28±2°C at 120 rpm. The fungal biomass collected after each day was dried and weighed to obtain the growth curve [20]

2.11. Epoxy resin coating set-up.

A mixture of epoxy resin and copper chloride nanoparticles was prepared, and a thin layer was coated onto a copper workpiece to check for the anti-corrosive property of the copper chloride-coated copper workpiece. For additional experimental use, all of the workpieces were stored in a desiccator for 72 h. For bacterial and fungal treatment, dried coated copper workpieces were submerged in MSM and M1 broth, respectively, exposed for 168 h while being shaken at 121 rpm and 37°C. Dry samples were examined for topological alterations using a scanning electron microscope [26].

2.12. Statistics.

Using Design type I Optimal and Quadratic model designs, a standard analysis of variance (ANOVA) was carried out. The threshold for statistical significance was established at $p = 0.05$.

3. Results and Discussion

3.1. Potent strain identification.

The bacterial isolate was identified as Gram-positive, aerobic, rod-shaped, catalase-producing, motile, and oxidase-positive bacteria based on preliminary biochemical assays. The findings of the biochemical characterisation are reported in Table 1. The presence of fused conidiospores was verified by lactophenol cotton blue staining. Figure S1 (a), (b), (c), and (d) illustrate conidiospore and hyphae production under a 100X light microscope (d). *Bacillus pacificus* 2JA is a catalase-producing bacterium. Biochemical characterisation has been tabulated in Table 1. The sequence was aligned and compared to the GenBank database. *Bacillus pacificus* 2JA and *Paecilomyces variotii* 2JA exhibited >99% homology in the results.

A BLAST search was used to determine the phylogenetic connection between the sequences. The cluster-tree analysis of the association between isolates and related species is shown in Figure S1. Both isolates' gene sequences were submitted to GenBank, where they were assigned the accession numbers MZ713004 and MZ702633, respectively.

Table 1. Biochemical tests for the preliminary identification of a bacterial isolate.

S.No.	Biochemical tests	*Bacillus pacificus* 2JA
1	MR	+
2	VP	-
3	Indole test	-
4	Citrate utilisation	-
5	TSI	Alk/Pink
6	SIM	-
7	Urease	-
8	Carbohydrate fermentation Sucrose Lactose Maltose Glucose	 - + - +
9	Oxidase	-
10	Catalase	+
11	Gelatin liquefaction	-
12	Nitrate reduction	+

'+' positive; '-' negative

This isolate generates a bacterial catalase enzyme to neutralise the cells during the synthesis of bacterial metabolites, which results in oxygen and the oxidation of metal ions. Catalase-mediated corrosion is the name given to this process [27]. The Fenton reaction is aided by the bacterial biofilm, which reduces metal ions, resulting in the generation of hydroxyl radicals (eq 2). The Cu^{2+} ions generated by the process combine with OH– ions to form copper oxide (eq. 3), which acts as a corrosion product on metal surfaces.

$$Cu^{2+} + H_2O_2 \rightarrow Cu^{2+} + 2OH \quad (2)$$

$$Cu^{2+} + 2H_2O \rightarrow Cu(OH)_2 \quad (3)$$

3.2. Microbial-mediated corrosion of copper workpiece.

Microbially influenced corrosion (MIC) occurred as a result of microbial metabolites that altered local chemistry and utilized copper ions from the metal surface to support microbial growth, thereby promoting corrosion. Tables 2, 3, and 4 present the weight loss (WL) and corresponding corrosion rate (CR) of copper coupons subjected to bacterial and fungal exposure. Following 14 days (336 h) of exposure, the average WL and CR for bacterial treatment were 2.6 ± 0.6 g and 0.0352 ± 0.1 mm/year, respectively, while fungal treatment resulted in a CR of 0.0238 ± 0.1 mm/year. At earlier time points, Cu coupons showed a CR of 0.0081 ± 0.2 mm/year (bacteria) and 0.033 ± 0.2 mm/year (fungi) after 6 h, which increased to 0.016 ± 0.5 mm/year and 0.039 ± 0.5 mm/year, respectively, by 48 h. Interestingly, the fungal CR decreased to 0.007 ± 0.1 mm/year by 168 h, likely due to the formation of a copper oxide re-passivation layer that inhibited further corrosion. A similar trend was observed in the bacterial trial, where initial corrosion rates were higher, possibly due to biofilm formation and direct contact of sessile cells with the metal surface. Over time, protective layers may have formed, leading to decreased metal–microbe interaction and a subsequent reduction in CR. The WL of bacterially treated coupons remained consistently higher than that of fungal-treated ones across the exposure period. These trends support the dynamic interplay between microbial

activity, oxide layer formation, and corrosion progression and are consistent with previously reported observations.XRD data from the corrosion product of bacterial-treated copper and fungal-treated metal workpiece are presented in Figure 1. CuO, Cu_2O_3, and $CaCO_3$ were observed in treated samples. CuO, Cu_2O_3, and $CaCO_3$ intensities decreased when the exposure length was increased, indicating a faster rate of corrosion on the metal workpiece. The re-passivation of the surface coating generated on the metal surface caused this event, which lasted until the conclusion of the exposure time. This behaviour persisted till the completion of the 336h exposure period.

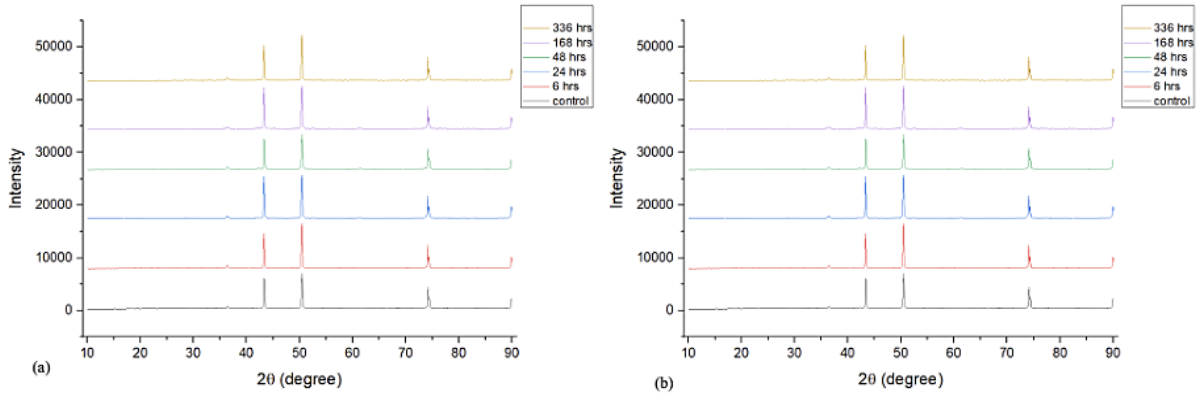

Figure 1. (a) XRD chromatogram of bacterial-treated copper coupons at 6, 24, 48, 168, and 336 h; **(b)** XRD chromatogram of fungal-treated copper coupons at 6, 24, 48, 168, and 336 h

Table 2. Weight loss occurred post-microbial trials.

Incubation days	Bacterial trial		Fungal trial	
	Control (g)	Treated (g)	Control (g)	Treated (g)
1st	2.855	2.842	2.975	2.883
3rd	2.802	2.613	2.644	2.563
7th	2.852	2.343	2.732	2.402

Table 3. Weight loss and corrosion rate data for the copper workpiece at different exposure times for the bacterial trial.

Hours	WL (g)	CR (mm/year)
6	0.003	0.0081
24	0.013	0.016
48	0.189	0.08
168	0.679	0.039
336	1.155	0.033

Table 4. Weight loss and corrosion rate data for the copper workpiece at different exposure times for the fungal trial.

Hours	WL (g)	CR (mm/year)
6	0.0019	0.003
24	0.092	0.039
48	0.221	0.038
168	0.402	0.023
336	0.567	0.016

3.3. Cu nanoparticle synthesis and characterisation.

The synthesis of copper chloride nanoparticles was confirmed with the deposition of dark brick colored clusters, as shown in Figure S4, which was dried and calcined to obtain the copper chloride nanoparticles. The characterisation of nanoparticles was done using XRD and SEM analysis. An X-ray chromatogram is depicted in Figure S5 with distinguished peaks confirming the powder to be a monoclinic structure of copper chloride. The average size of the

synthesized $CuCl_2$ powder was calculated using the Debye-Scherrer equation (equation 4), which is explained as:

$$D = \frac{K\lambda}{\beta Cos\Theta} Å \qquad (4)$$

Where D = average crystalline size (in Å), K = shape factor (0.9), λ = Wavelength of X-Ray (1.5406 Å), Θ = Bragg angle, and β = corrected line broadening of the nanoparticles.

The particle size was calculated using the above-mentioned formula and was found to be 42.5 nm. The SEM chromatogram showed round-shaped copper chloride nanoparticles that agglomerated to form clusters of balls. The EDAX spectrum shows the presence of copper, thus confirming the synthesis of copper oxide nanoparticles as shown in Figure S8.

All control experiments, including uncoated, epoxy-only, and microbe-only treatments, were conducted under identical incubation conditions (37°C, 121 rpm, and respective media) to ensure valid comparative analysis.

Figure 2 shows the establishment of a bacterial biofilm and its growth over time in SEM images of bacterial and fungal-treated Cu coupons at varying exposure durations. MIC occurs simultaneously with the creation of EPSs and cellular attachment to the metal surface during biofilm development.

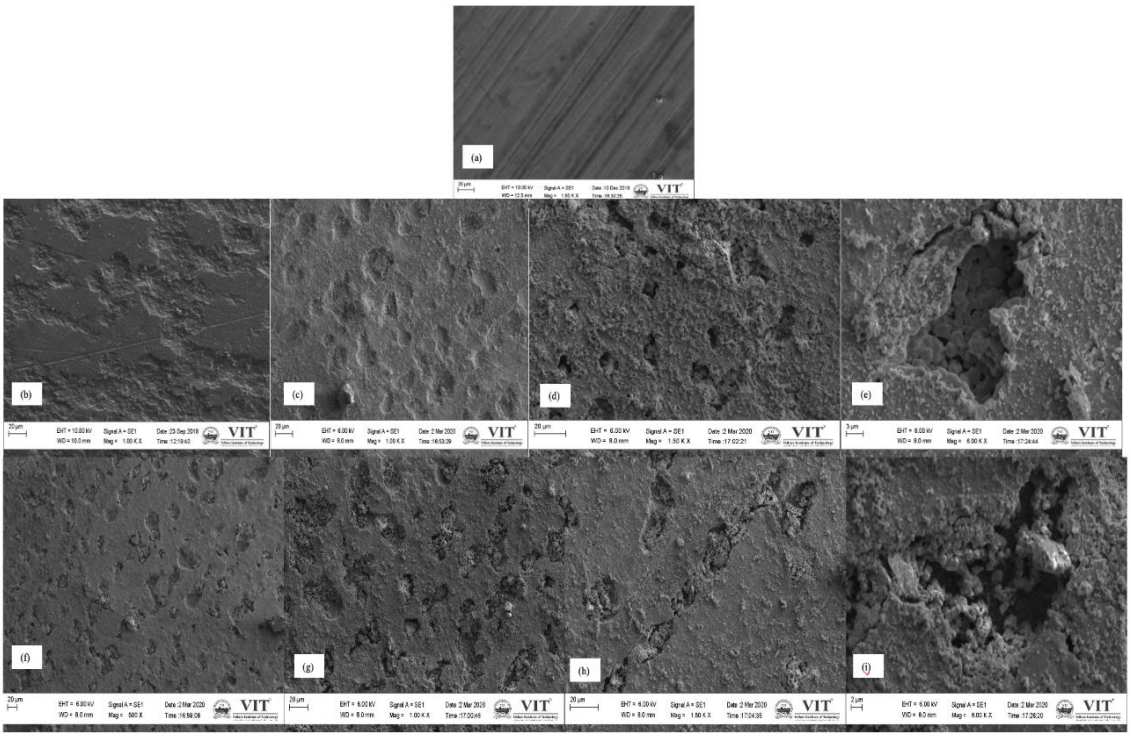

Figure 2. (a) Control SEM chromatogram of Cu workpiece showing smooth surface devoid of any corrosion; **(b)** Micrographs depicting formation of multiple pits on the metal surface post 168 h of bacterial trial taken at different magnification scales of 500x, 1000x, 1500x, and 6000x. At 6000x, there is colonisation of bacteria inside the pits formed on metal surfaces; **(f)** Micrographs depicting formation of multiple pits on the metal surface post 168 h of fungal treatment taken at different magnification scales of 500x, 1000x, 1500x, and 6000x. Magnification of 1500x shows a trail of pits leading to the formation of cracks post longer exposure. At 6000x, there is an agglomeration of fungal mycelium inside the pits formed on a metal surface.

These activities cause a considerable change in the metal interface, which serves as a barrier to element swapping between the aqueous phase and the metal surface [27]. The increased generation of EPSs on the metal surface causes differential aeration and changes in

pH and redox reactions (potential difference) on the metal surfaces, resulting in corrosion [28]. Due to instrumentation constraints, FTIR and XPS analyses could not be performed; future studies are encouraged to employ these techniques for detailed surface chemistry and oxide characterization.

Post incubation of 6 h, 24 h, 48 h, 168 h, and 336 h the flasks containing bacterial and fungal isolate were taken out as shown in figures S2 (a), (b), (c), (d) and metal pieces were dried in overnight in an oven at 55°C for further surface analysis using SEM. AFM chromatograms of typical pits on corroded coupons at varied periods. Atomic Force Microscopy (AFM) revealed progressive pit formation on copper coupon surfaces over time. At 168 h of microbial exposure, the mean pit depths were 144.24 ± 28.67 nm for bacterial treatment and 152.31 ± 12.03 nm for fungal treatment. With extended exposure up to 336 h, the depth increased significantly to 397.02 ± 48.40 nm for bacterial and 304.78 ± 23.68 nm for fungal trials (Table 5). AFM images at 25 µm confirmed these findings, and early-stage micro-pitting (~150 nm) was observed at 168 h. Notably, copper coupons treated with copper chloride nanoparticles or coated with epoxy-nanoparticle mixtures showed no detectable pit formation, maintaining smooth topographies throughout the exposure period (as shown in Figure S10 (a) and (b)).

Table 5. Mean calculated depth of pit on the Cu coupons post bacterial and fungal trial for 168 and 336 h of exposure.

Exposure time (h)	Depth (mm)	
	Bacteria	Fungus
168	144.24 ± 28.67	152.31± 12.03
336	397.02 ± 48.40	304.78 ± 23.68

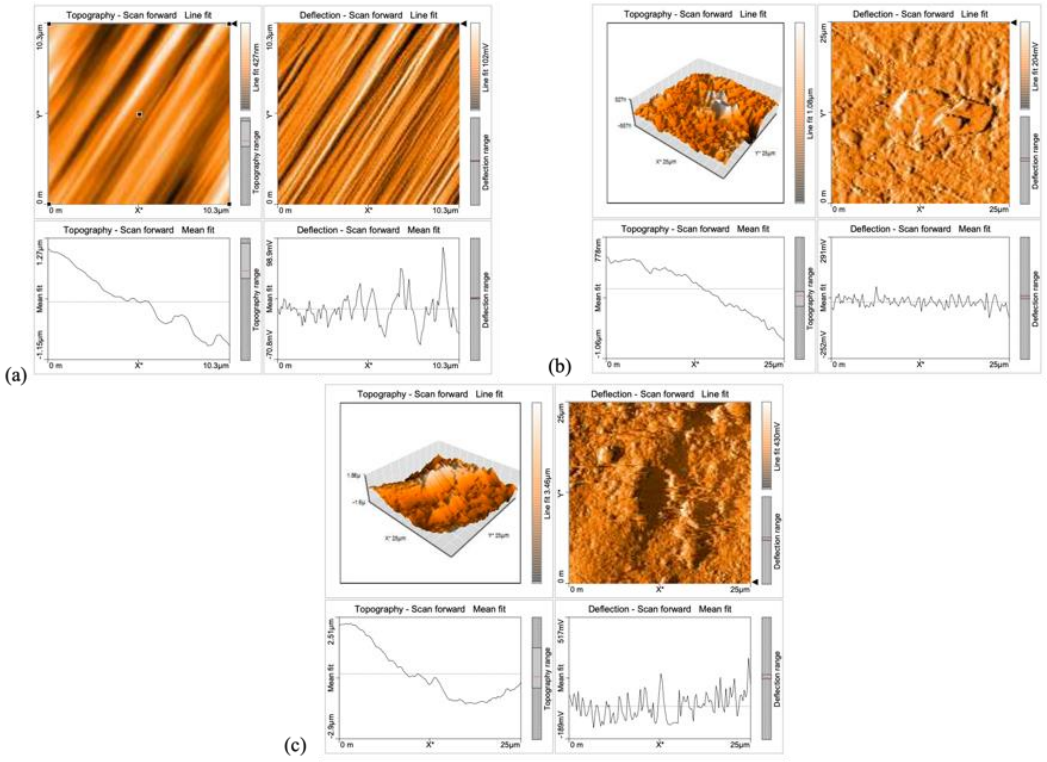

Figure 3. (a) Control AFM chromatogram of control copper coupon of 1.0 cm x 1.0 cm x 0.3 cm in size analysed at 10µm; **(b)** AFM chromatogram showing pit formation on scanned topographical graph at 25 µm post fungal treatment of copper at 336 h; **(c)** AFM chromatogram showing pit formation on scanned topographical graph at 25 µm post bacterial treatment of copper at 336 h.

After the biofilms and deposits were removed, the level of corrosion damage induced by bacterial colonisation was determined by profiling the pits on the coupon surface. Figure 3 shows the AFM chromatogram of the control coupon surface after 168 and 336 h of exposure to the liquid media without microbes. After 336 h of exposure, there are no pits visible on the control coupons. As shown in Figure 4, a control coupon had a smooth and pit-free surface (a). Pitting corrosion was discovered on the coupon surface after a 336h trial period, and the number of pits and their diameters increased with time (Figure 3(b)–(c) and Figure S11).

[2728]To compare the anti-corrosive effectiveness of each treatment, a quantitative analysis of corrosion rates at 168 h was compiled (Table 6). The results confirm the synergistic benefit of combining copper chloride nanoparticles with epoxy coatings for maximum protection.

Table 6. Corrosion rate comparison of copper coupons under different treatments at 168 h exposure.

Microbial strain	Treatment condition	Corrosion rate (mm/year)	Corrosion rate reduction (%) vs. untreated microbial trial
Bacillus pacificus 2JA	Copper + Bacteria (no treatment)	0.039	-
	Copper + Bacteria + $CuCl_2$ Nanoparticles	0.003783	90.3%
	Copper + Bacteria + Epoxy + $CuCl_2$ Nanoparticles	~0.000 (no pits observed)	~100%
Paecilomyces variotii 2JA	Copper + Fungus (no treatment)	0.023	-
	Copper + Fungus + $CuCl_2$ Nanoparticles	0.012105	47.3%
	Copper + Fungus + Epoxy + $CuCl_2$ Nanoparticles	~0.000 (no pits observed	~100%

3.4. MIC of copper chloride nanoparticle.

Well diffusion was performed to detect the MIC of copper chloride nanoparticles. The nanoparticles were able to inhibit bacterial growth at a concentration of 1 mg/ml. $CuCl_2$ nanoparticles were effective due to the greater surface area of the nanoparticles. The positively charged nanoparticles will attach to the negatively charged surface of the microbes and thus show toxicity against the organisms [29]. From the zone of inhibition value, a concentration of 1 mg/mL was used for further anti-corrosive test analysis, as shown in Figure S9.

3.5. Growth kinetics of potent bacterial and fungal isolates.

The growth pattern of the bacterial isolate was studied by measuring the optical densities at 600 nm at a regular interval of time of 24 h. The inoculation suspension of bacterial culture was 10^{-6} CFU/ml. The initial absorbance value recorded was almost negligible; it increased after 10 min of incubation in the case of both organisms. After 5 h of incubation, the rapid growth of both bacterial isolates was exhibited. Hence, the growth of bacteria from 0-5 h was observed as a lag phase as depicted in Figure S3(a) and (b). The exponential phase was observed at 5 h with rapid cell growth. Growth continued to increase till 15 h, followed by attaining stability. The stable growth of both bacterial isolates depicts the stationary phase, as there was no net growth of bacteria. The growth curve of fungal strains depicts that the isolate showed the highest growth till the 5^{th} day, as shown in Figure S3 (b). MIC of the copper chloride nanoparticles is shown in Figures S8 and S9.

3.6. Anti-corrosion nature of copper chloride nanoparticle.

A scanning electron micrograph was used to detect the morphological changes occurring on the metal pieces inoculated with $CuCl_2$ nanoparticles and cultures. After 14 days of incubation of the metal with nanoparticles, less corrosion was observed as compared to the previous trials. The copper chloride nanoparticles inhibited the growth of the bacterial and fungal isolates in the media, thereby inhibiting the biofilm and mycelial mat formation on the surface of the metal workpiece, according to a study conducted by Lai *et al*. [30]. This inhibition was attributed to metal ion toxicity via Cu^{2+} uptake, which disrupts enzyme function and oxidative phosphorylation. The electrostatic interactions between positively charged $CuCl_2$ nanoparticles and negatively charged potent microbial strains lead to membrane destabilisation [31]. Also, ROS generation, including hydroxyl radicals, causes oxidative damage to the cellular macromolecules of the bacterial or fungal isolates [32].

The positive charge of $CuCl_2$ nanoparticles results in electrostatic interaction with the negatively charged microbial cells, resulting in the adhesion of the organisms to the particles [33]. Once the particles are attached to the organisms, reactive oxygen species are released, which disrupt the cell walls, causing cell death [34]. Thus, the copper chloride nanoparticles are capable of protecting the metal workpiece from the corrosion activity of the bacterial and fungal strains.

3.7. Epoxy resin coating set-up.

Post 168 h of the incubation period, both bacterial- and fungal-treated copper workpieces were washed with distilled water, and surface topology was analysed using the scanning electron microscope. There were no pitting or conformational changes on the workpiece as shown in Figure 4 and AFM in Figure S10. The findings obtained suggested that the coating has remarkably improved the anti-corrosion performance. Additionally, the corrosion-protecting effects of the coating process were investigated using scanning electron microscopy analysis. Scanning electron microscopy observations confirm that the coating is regarded as a protective layer on copper surfaces.

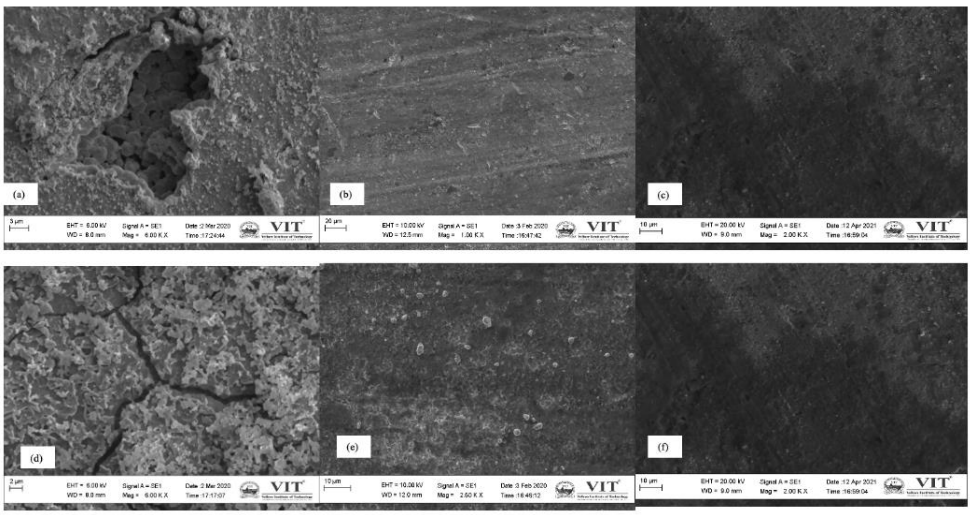

Figure 4. (a) SEM micrograph of 14th day bacterial trial; **(b)** SEM micrograph showing no pit formation with $CuCl_2$ nanoparticle trial inhibiting the growth of *Bacillus pacificus* 2JA isolate; **(c)** Epoxy resin coating on workpiece with no bacterial growth; **(d)** SEM micrograph of 14th day fungal trial; **(e)** SEM micrograph showing no pit formation with $CuCl_2$ nanoparticle trial inhibiting the growth of *Paecilomyces variotii* 2JA isolate; **(f)** Epoxy resin coating on workpiece with no fungal growth.

3.8. Statistical analysis.

The ANOVA prediction was made using a quadratic model. Weight loss and corrosion rate are two reactions that have been connected, and the results have been measured for copper sample behaviour.

Experimental design (DOE) has been tabulated in Tables 7 and 8. The duration of corrosion, exposure to bacteria and fungus, and exposure to various concentrations of copper chloride nanoparticles (0.5 mg/L, 1.0 mg/L, and 1.5 mg/L) are among the aspects that were examined. From the ANOVA Table 7, the regression cubic equations (equations 5 and 6) formed were:

$$Microbes : Bacteria \Longrightarrow Corrosion\,rate = 0.011008 - 0.008158\,A + 0.00004\,B - 0.000013\,AB \quad (5)$$

$$Microbes : Fungi \Longrightarrow Corrosion\,rate = 0.016321 - 0.009952\,A + 0.000033\,B - 0.000013\,AB \quad (6)$$

Table 7. Factors, levels, and responses of a full factorial experimental design.

Std order	Factor 1	Factor 2	Factor 3	
	A: Nanoparticles	B: Duration of corrosion	Corrosion rate (mm/year)	
	mg/L	Hours	C: Bacteria	C: Fungi
1	0	6	0.0081	0.003
2	0.5	6	0.006518	0.001629
3	1	6	0.004888	0.001629
4	1.5	6	0.004888	0.001629
5	0	24	0.016	0.039
6	0.5	24	0.002037	0.004074
7	1	24	0.001629	0.003259
8	1.5	24	0.001629	0.002852
9	0	48	0.005	0.038
10	0.5	48	0.004074	0.006111
11	1	48	0.003666	0.005703
12	1.5	48	0.003463	0.005296
13	0	168	0.039	0.023
14	0.5	168	0.003841	0.012221
15	1	168	0.003783	0.012105
16	1.5	168	0.003724	0.011988
17	0	336	0.033	0.016
18	0.5	336	0.008118	0.012628
19	1	336	0.00806	0.01257
20	1.5	336	0.008031	0.01257

Table 8. ANOVA for full factorial design.

Source	Sum of squares	df	% contribution	p-value
Model	0.0027	8	62.8	< 0.0001*
A-Nanoparticles	0.0021	3	48.8	< 0.0001*
B-Duration of corrosion	0.0007	4	16.3	0.0169*
C-Microbes	0.0001	1	2.3	0.1098
Residual	0.0015	31	34.9	
Cor Total	0.0043	39		

*Significantly influencing the output

The quadratic model supported the study and showed a 62.8% contribution. P-value was found to be <0.0001, significantly influencing the output. A proper fit line was obtained from regression analysis (Figure S6). The response surface 3D plot concludes that *Bacillus pacificus* 2JA and *Paecilomyces variotii* 2JA showed a higher corrosion rate when compared to exposure to copper chloride nanoparticles. These nanoparticles can be synthesised in bulk and used as an anti-corrosive coating over copper metal.

The ANOVA results demonstrated that nanoparticle concentration had a statistically significant effect on corrosion rate ($p < 0.0001$), accounting for 48.8% of the variation. Duration of exposure also showed a significant influence ($p = 0.0169$), contributing 16.3%. Although microbial type (bacteria vs. fungi) contributed 2.3%, it was not statistically significant ($p = 0.1098$), indicating comparable corrosive behavior between the strains. The interaction term (AB) between nanoparticle concentration and exposure duration was statistically relevant, confirming a synergistic effect on corrosion mitigation. The overall model showed a good fit with an adjusted R^2 of 62.8%, supporting the robustness of the experimental design. These findings underscore the dominance of nanoparticle concentration as a controllable factor in microbial corrosion prevention.

With the limited data available (duration, microbial exposure, and nanoparticle exposure), an effective model was designed to support the present study. A quantitative 3D bar plot has been depicted in Figure 5. The interaction plot depicted in Figure S7 showed the effect of copper chloride nanoparticles on various durations of corrosion periods of 24h, 48h, 168h, and 336h.

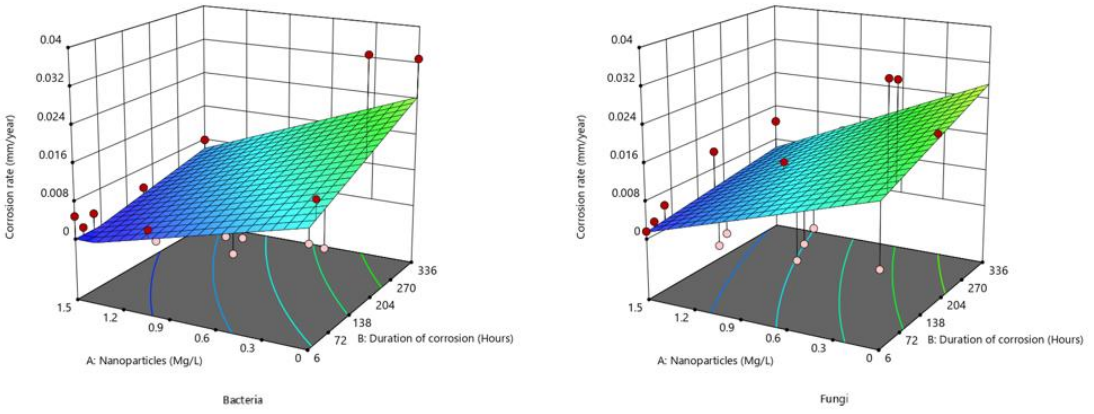

Figure 5. Quantitative information through a 3D bar chart.

It can be observed that nanoparticles at 1.5 mg/L concentration showed a lesser corrosion rate, thereby inhibiting the growth of both the isolates, whereas at 0.5 mg/L concentration, the corrosion rate is much higher with respect to bacterial and fungal isolates. Similarly, in Figure 6, the corrosion due to nanoparticles is significantly less than that induced by both bacterial and fungal isolates.

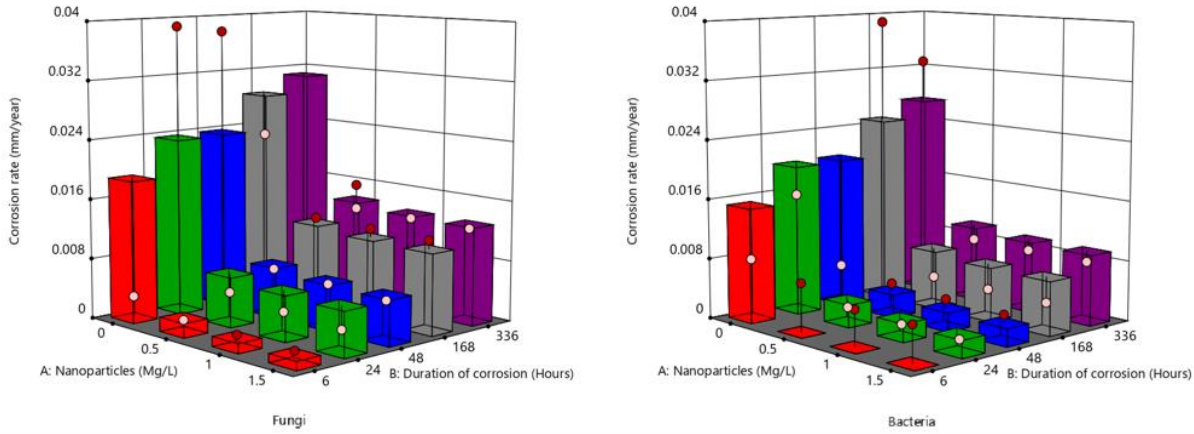

Figure 6. Surface plot that shows the effect of nanoparticles and the duration of corrosion.

4. Conclusions

The function of copper chloride nanoparticles' anti-corrosion action on copper coupons was examined in this work. The corrosive bacteria and fungus species *Bacillus pacificus* 2JA and *Paecilomyces variotii* 2JA were discovered, and corrosion studies on metal surfaces were conducted using WL, XRD, SEM, and AFM. The existence of CuO, Cu_2O_3, and Ca oxide as corrosion products was verified by XRD. The isolated bacterial and fungal strains were able to convert the elements on the copper coupon surfaces, indicating that they are capable of doing so. Atomic force microscopic pictures helped to confirm the result. The findings showed that, owing to bacterial metabolism, bacterial and fungal isolates increase the corrosion of Cu coupons. The WL experiment demonstrated that bacterially treated samples are more corrosion resistant than fungal-treated coupons. Copper chloride nanoparticles showed a good anti-corrosion ability and can be produced in bulk as a coating design material. From the quadratic model study, the adjusted R^2 value was found to be 62.8%. The present study confirms the common fact that the corrosion rate is directly proportional to the duration of corrosion, which is 16.3% influential on the corrosion rate. In conjunction with this fact, it is found that the synthesized copper chloride nanoparticle showed 48.8% influence in controlling the corrosion rate. In addition, the interaction effect of microbes (fungi and bacteria) and the duration of corrosion had a 2.3% influence on the corrosion rate. The bacterial community promotes the corrosion of copper metal used in many technical applications. While antimicrobial efficacy was confirmed against pathogenic bacteria, future studies should assess the potential ecotoxicological effects of copper sulphate nanoparticles on non-target organisms and environmental systems. This research contributes to the advancement of existing understanding of the role of copper chloride nanoparticles in corrosion prevention. It can be employed as biocides or corrosion inhibitors in the processing industry.

Author contributions

Conceptualization, J.A.; methodology, J.A.; formal analysis, J.A.K.; investigation, J.A.K.; data curation, J.A. and M.S.; writing—original draft preparation, J.A., M.S., and A.S.; writing—review and editing, J.A.; visualization, J.A.K.; supervision, J.A.; All authors have read and agreed to the published version of the manuscript.

Institutional Review Board Statement

Not applicable.

Informed Consent Statement

Not applicable.

Data Availability Statement

The data supporting the findings of this study are available upon reasonable request from the corresponding author.

Funding

The authors declare that no funds, grants, or other support were received during the preparation of this manuscript.

Acknowledgment

The authors would like to express their gratitude to the management of VIT, Vellore.

Conflict of interest

The authors have no conflict of interest to declare.

References

1. Tan, B.; Zhang, S.; Qiang, Y.; Guo, L.; Feng, L.; Liao, C.; Xu, Y.; Chen, S. A Combined Experimental and Theoretical Study of the Inhibition Effect of Three Disulfide-Based Flavouring Agents for Copper Corrosion in 0.5 M Sulfuric Acid. *J. Colloid Interface Sci.* **2018**, *526*, 268–280, https://doi.org/10.1016/j.jcis.2018.04.092.
2. Zhao, J.; Csetenyi, L.; Gadd, G. M. Biocorrosion of Copper Metal by Aspergillus Niger. *Int Biodeterior Biodegradation* **2020**, *154*, 105081, https://doi.org/10.1016/j.ibiod.2020.105081.
3. Mehta, K. D.; Das, C.; Pandey, B. D. Leaching of Copper, Nickel and Cobalt from Indian Ocean Manganese Nodules by Aspergillus Niger. *Hydrometallurgy* **2010**, *105*, 89–95, https://doi.org/10.1016/j.hydromet.2010.08.002.
4. Sette, L. D.; Passarini, M. R. Z.; Rodrigues, A.; Leal, R. R.; Simioni, K. C. M.; Nobre, F. S.; de Brito, B. R.; da Rocha, A. J.; Pagnocca, F. C. Fungal Diversity Associated with Brazilian Energy Transmission Towers. *Fungal Divers* **2010**, *44*, 53–63, https://doi.org/10.1007/s13225-010-0048-y.
5. Liduino, V.; Galvão, M.; Brasil, S.; Sérvulo, E. SRB-Mediated Corrosion of Marine Submerged AISI 1020 Steel under Impressed Current Cathodic Protection. *Colloids Surf. B Biointerfaces* **2021**, *202*, 111701, https://doi.org/10.1016/j.colsurfb.2021.111701.
6. Liang, R.; Li, J.; Liu, M.; Huang, Z. Y. Influence of Inhibitors on the Adhesion of SRB to the Stainless Steel in Circulating Cooling Water. *Colloids Surf. B Biointerfaces* **2018**, *172*, 1–9, https://doi.org/10.1016/j.colsurfb.2018.08.013.
7. Amendola, R.; Acharjee, A. Microbiologically Influenced Corrosion of Copper and Its Alloys in Anaerobic Aqueous Environments: A Review. *Fron Microbiol.* **2022**, *13*, 806688, https://doi.org/10.3389/fmicb.2022.806688.
8. Zhu, H.; Li, X.; Lu, X.; Wang, J.; Hu, Z.; Ma, X. Efficiency of Gemini Surfactant Containing Semi-Rigid Spacer as Microbial Corrosion Inhibitor for Carbon Steel in Simulated Seawater. *Bioelectrochemistry* **2021**, *140*, 107809, https://doi.org/10.1016/j.bioelechem.2021.107809.
9. Dong, Z. H.; Liu, T.; Liu, H. F. Influence of EPS Isolated from Thermophilic Sulphate-Reducing Bacteria on Carbon Steel Corrosion. *Biofouling* **2011**, *27*, 487–495, https://doi.org/10.1080/08927014.2011.584369.
10. Zarasvand, K.A.; Rai, V.R. Microorganisms: Induction and Inhibition of Corrosion in Metals. *Int Biodeterior Biodegradation* **2014**, *87*, 66–74, https://doi.org/10.1016/j.ibiod.2013.10.023.
11. Xu, Z.; Dou, W.; Chen, S.; Pu, Y.; Chen, Z. Limiting Nitrate Triggered Increased EPS Film but Decreased Biocorrosion of Copper Induced by Pseudomonas Aeruginosa. *Bioelectrochemistry* **2022**, *143*, 107990, https://doi.org/10.1016/j.bioelechem.2021.107990.
12. Hu, Y.; Xiao, K.; Yan, L.; Hao, X.; Huang, L.; Lou, Y. Effect of Fungus, Aspergillus Sp. F1-1, on the Corrosion Behavior of PCB-HASL in Humid Atmospheric Environment. *Surf. Topogr.: Metrol. Prop.* **2022**, *10*, 015022, https://doi.org/10.1088/2051-672X/ac459b.
13. Wang, J.; Xiong, F.; Liu, H.; Zhang, T.; Li, Y.; Li, C.; Xia, W.; Wang, H.; Liu, H. Study of the Corrosion Behavior of Aspergillus Niger on 7075-T6 Aluminum Alloy in a High Salinity Environment. *Bioelectrochemistry* **2019**, *129*, 10–17, https://doi.org/10.1016/j.bioelechem.2019.04.020.
14. Farag, A. A.; Abdallah, H. E.; Badr, E. A.; Mohamed, E. A.; Ali, A. I.; El-Etre, A. Y. The Inhibition Performance of Morpholinium Derivatives on Corrosion Behavior of Carbon Steel in the Acidized

Formation Water: Theoretical, Experimental and Biocidal Evaluations. *J. Mol. Liq.* **2021**, *341*, 117348, https://doi.org/10.1016/j.molliq.2021.117348.
15. Chen, S.; Deng, H.; Zhao, Y.; Lu, S.; Zhao, Y.; Cheng, X.; Liu, G.; Dou, W.; Chen, J. The Effects of Methanococcus Maripaludis on the Corrosion Behavior of EH40 Steel in Seawater. *Bioelectrochemistry* **2021**, *140*, 107824, https://doi.org/10.1016/j.bioelechem.2021.107824.
16. Chakraborty, P.; Abraham, J. Comparative Study on Degradation of Norfloxacin and Ciprofloxacin by Ganoderma Lucidum JAPC1. *Korean J. Chem. Eng.* **2017**, *34*, 1122–1128, https://doi.org/10.1007/s11814-016-0345-6.
17. Chatterjee, A.; Abraham, J. Desorption of Heavy Metals from Metal Loaded Sorbents and E-Wastes: A Review. *Biotechnol. Lett.* **2019**, *41*, 319–333, https://doi.org/10.1007/s10529-019-02650-0.
18. Parameswaran, P.; Rameshbabu, A. M.; Krishnan, G. N.; Yogeshwaran, R.; Ramkumar, R. Study of the Corrosion Properties in a Hot Forged Cu-Al-Ni Alloy with Added Cr. *J. Mech. Behav. Mater.* **2018**, *27*, 3–4, http://dx.doi.org/10.1515/jmbm-2018-0016.
19. Rajasekar, A.; Ting, Y.-P. Microbial Corrosion of Aluminum 2024 Aeronautical Alloy by Hydrocarbon Degrading Bacteria Bacillus Cereus ACE4 and Serratia Marcescens ACE2. *Ind. Eng. Chem. Res.* **2010**, *49*, 6054–6061, http://dx.doi.org/10.1021/ie100078u.
20. Chatterjee, A.; Abraham, J. Mycoremediation of 17 B-Estradiol Using Trichoderma Citrinoviride Strain AJAC3 along with Enzyme Studies. *Environ. Prog. Sustain. Energy* **2019**, *38*, 13142, https://doi.org/10.1002/ep.13142.
21. Kodama, Y.; Tomioka, N.; Ito, M.; Imae, N. Developments in Microfabrication of Mineral Samples for Simultaneous EBSD–EDS Analysis Utilizing an FIB–SEM Instrument: Study on an S–Type Cosmic Spherule from Antarctica. *J. Mineral Petrol Sci.* **2020**, *115*, 407–415, https://doi.org/10.2465/jmps.181227.
22. Fontana, M.G.; Corrosion Engineering, 1st Edition; McGraw Hill: **1967**.
23. Döşlü, S.T.; Mert, B.D.; Yazıcı, B. The Electrochemical Synthesis and Corrosion Behaviour of TiO2/Poly (Indole-Co-Aniline) Multilayer Coating: Experimental and Theoretical Approach. *Arab J Chemi.* **2018**, *11*, 1–13. https://doi.org/10.1016/j.arabjc.2017.03.007.
24. Umer, A.; Naveed, S.; Ramzan, N.; Rafique, M.S. Selection of a Suitable Method for the Synthesis of Copper Nanoparticles. *Nano* **2012**, *7*, 1230005, https://doi.org/10.1142/S1793292012300058.
25. Sadouk- Hachaïchi, Z.; Tazerouti, A.; Hacene, H. Growth Kinetics Study of a Bacterial Consortium Producing Biosurfactants, Constructed with Six Strains Isolated from an Oily Sludge. *Adv. Biosci. Biotechnol.* **2014**, *5*, 418-425, https://doi.org/10.4236/abb.2014.55050.
26. Zhang, C.; Dai, X.; Wang, Y.; Sun, G.; Li, P.; Qu, L.; Sui, Y.; Dou, Y. Preparation and Corrosion Resistance of ETEO Modified Graphene Oxide/Epoxy Resin Coating. *Coatings* **2019**, *9*, 46, https://doi.org/10.3390/coatings9010046.
27. Guo, N.; Zhao, Q.; Hui, X.; Guo, Z.; Dong, Y.; Yin, Y.; Zeng, Z.; Liu, T. Enhanced Corrosion Protection Action of Biofilms Based on Endogenous and Exogenous Bacterial Cellulose. *Corros. Sci.* **2022**, *194*, 109931, https://doi.org/10.1016/j.corsci.2021.109931.
28. Chang, T.; Butina, K.; Herting, G.; Rajarao, G. K.; Richter-Dahlfors, A.; Blomberg, E.; Wallinder, I. O.; Leygraf, C. The Interplay between Atmospheric Corrosion and Antimicrobial Efficiency of Cu and Cu5Zn5Al1Sn during Simulated High-Touch Conditions. *Corros Sci.* **2021**, *185*, 109433, https://doi.org/10.1016/j.corsci.2021.109433.
29. González, E.A.; Leiva, N.; Vejar, N.; Sancy, M.; Gulppi, M.; Azócar, M. I.; Gomez, G.; Tamayo, L.; Zhou, X.; Thompson, G. E. Sol–Gel Coatings Doped with Encapsulated Silver Nanoparticles: Inhibition of Biocorrosion on 2024-T3 Aluminum Alloy Promoted by Pseudomonas Aeruginosa. *J. Mater. Res. Technol.* **2019**, *8*, 1809–1818, https://doi.org/10.1016/j.jmrt.2018.12.011.
30. Lai, Y.; Gao, F.F.; Ge, R.T.; Liu, R.; Ma, S.; Liu, X. Metal ions overloading and cell death. *Cell Biol. Toxicol.* **2024**, *40*, 72, https://doi.org/10.1007/s10565-024-09910-4.
31. Malekkhaiat Häffner, S.; Malmsten, M. Interplay between Amphiphilic Peptides and Nanoparticles for Selective Membrane Destabilization and Antimicrobial Effects. *Curr. Opin Colloid Interface Sci.* **2019**, *44*, 59–71, https://doi.org/10.1016/J.COCIS.2019.09.004.
32. He, H.; Zou, Z.; Wang, B.; Xu, G.; Chen, C.; Qin, X.; Yu, C.; Zhang, J. Copper Oxide Nanoparticles Induce Oxidative DNA Damage and Cell Death via Copper Ion-Mediated P38 MAPK Activation in Vascular Endothelial Cells. *Int. J. Nanomed.* **2020**, *15*, 3291–3302, https://doi.org/10.2147/IJN.S241157.

33. Feng, F.; Pu, Y.; Hou, S.; Zhu, C.; Chen, S. Elucidating Different Microbiologically Influenced Corrosion Behavior of Copper, 90/10 Cu-Ni Alloy, 70/30 Cu-Ni Alloy and Nickel from the Perspective of Element Content. *Bioelectrochemistry* **2025**, *162*, 108854, https://doi.org/10.1016/j.bioelechem.2024.108854.
34. Al-Aifan, B.; Gouroju, N. K.; Gunamgari, B. R.; N, A.; Balam, D. P.; Gangarapu, S. R. Developing a Novel Copper Nano-Based Emulsified Cutting Fluid with Antimicrobial and Anticorrosion Properties–an Attempt for Sustainability. *Anti-Corrosion Methods and Materials* **2025**, *72*, 403–419, https://doi.org/10.1108/ACMM-07-2024-3046.

Publisher's Note & Disclaimer

Supplementary file

The sequence was aligned and compared to the GenBank database. *Bacillus pacificus* 2JA and *Paecilomyces variotii* 2JA exhibited >99% homology in the results. A BLAST search was used to determine the phylogenetic connection between the sequences. The cluster-tree analysis of the association between isolates and related species is shown in Figure S1. Both the isolates' gene sequences were submitted to GenBank, where they were assigned the accession number MZ713004 and MZ702633, respectively.

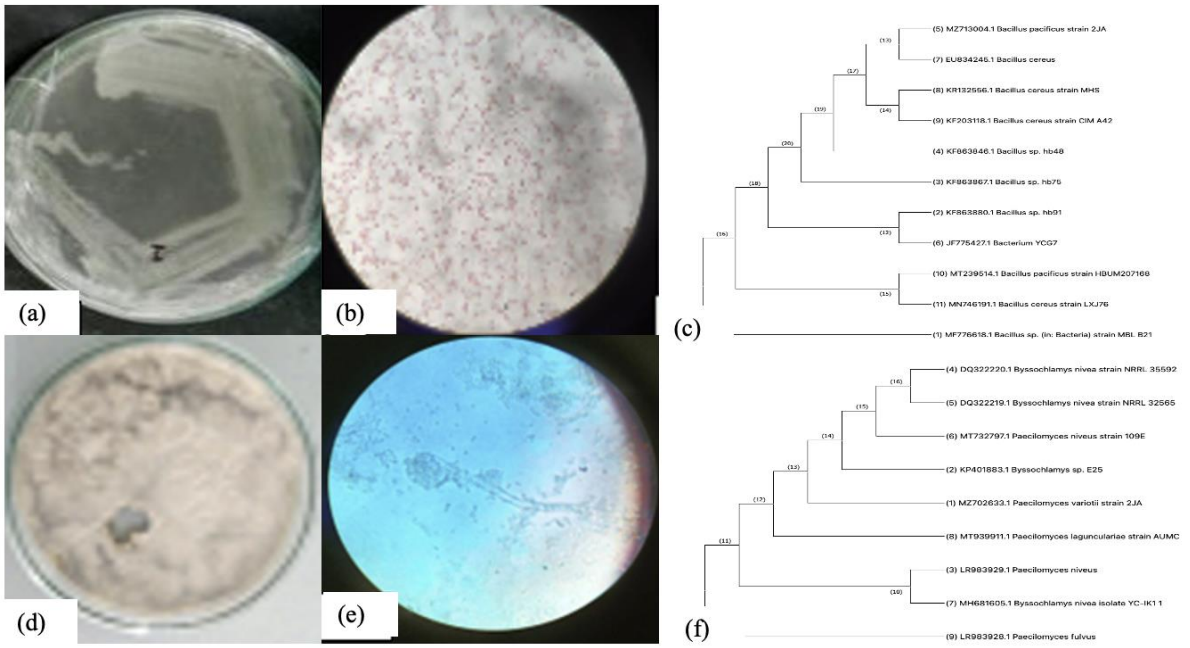

Figure S1. (a) bacterial isolate on nutrient agar, (b)Gram staining showing Gram positive rods, (c) Phylogenetic tree analysis using muscle alignment of *Bacillus pacificus* 2JA showing 99.9% similarity with *Bacillus* sp., (d) fungal isolate on potato dextrose agar medium, (e) LPCB staining and (e) Phylogenetic tree analysis using muscle alignment of *Paecilomyces variotii* 2JA showing 99.9% similarity with *Paecilomyces* sp.

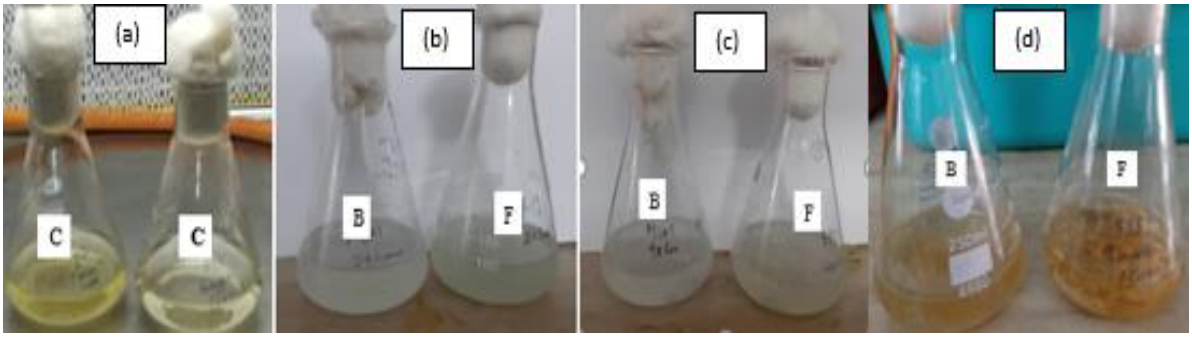

Figure S2. (a) Control flasks with copper workpiece in MSM and M1 medium; (b) 6 hrs of biocorrosion of copper trial; (c) 168 hrs of biocorrosion trial and (d) 336 hrs of biocorrosion trial.

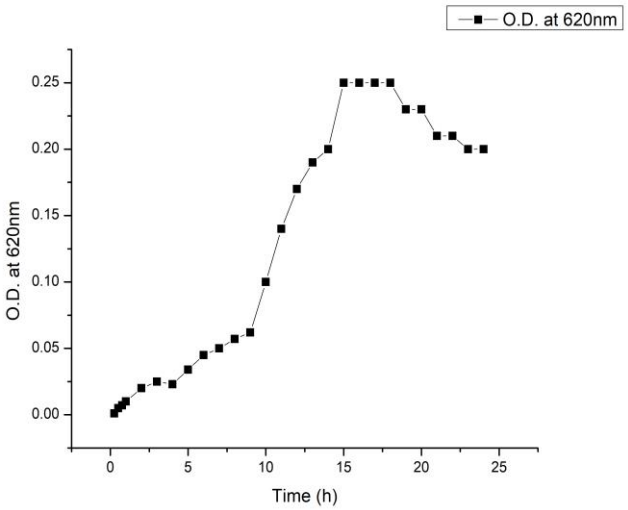

Figure S3. (a) Growth curve for bacterial isolate *Bacillus pacificus* 2JA.

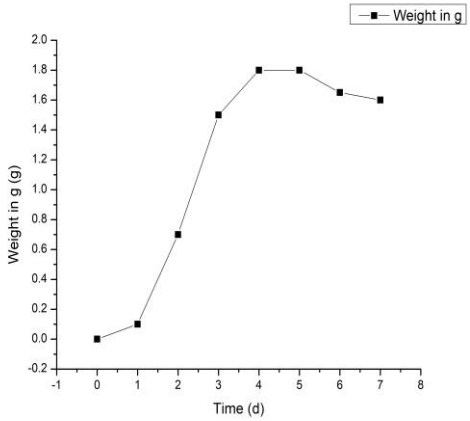

Figure S3. (b) Growth curve for fungal isolate *Paecilomyces variotii* 2JA

This phase marked the phenomenon where the increase in the count of cells was equal to the number of bacterial cell deaths. Post 20 h of incubation, negligible reduction of bacterial cell growth was observed which might be due to the depletion of the nutrients in the medium. The growth curve of the fungal culture was however checked for 7 d. The biomass was dried in an oven and the dry weight of the biomass was measured to obtain the fungal growth curve.

Figure S4. Synthesized copper chloride nanoparticles.

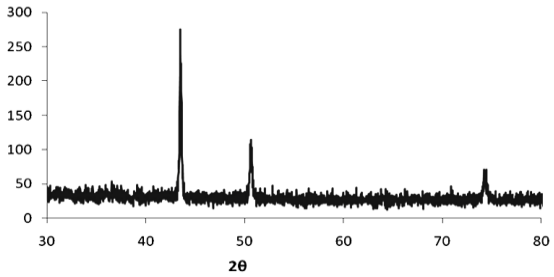

Figure S5. XRD analysis spectrum of the copper chloride nanoparticles.

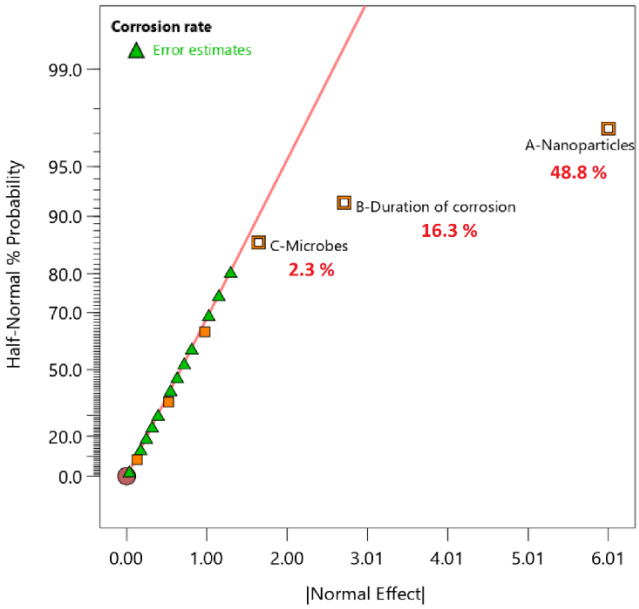

Figure S6. Half-normal percent probability plot.

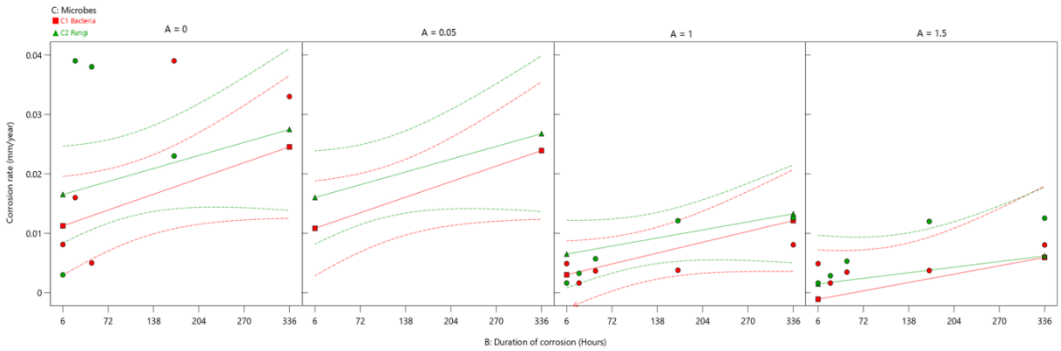

Figure S7. Interaction effect between nanoparticle versus duration of corrosion under different microbes.

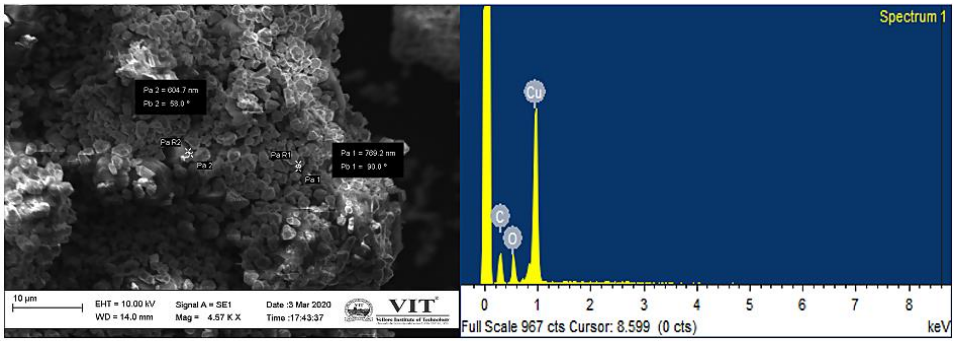

Figure S8. (a) SEM and (b) EDAX spectrum of copper chloride nanoparticles.

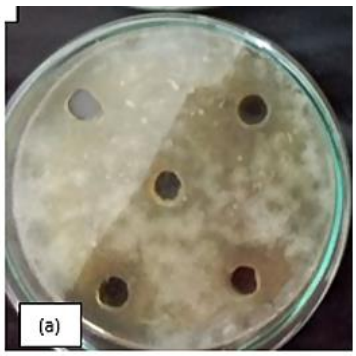

Figure S9. Antimicrobial activity of copper chloride nanoparticle at varying concentration.

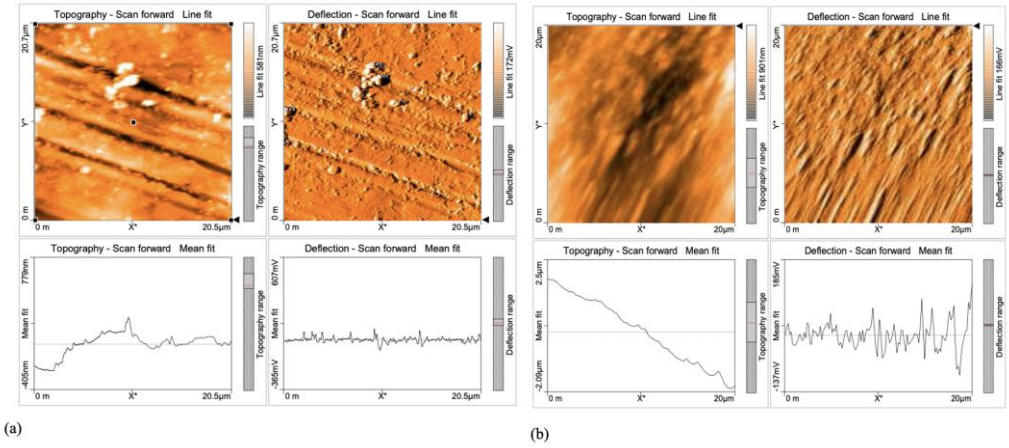

Figure S10. AFM chromatogram showing smooth surface post treatment with copper chloride nanoparticles and (a) 336 h of bacterial exposure and (b) 336 h of fungal exposure on copper coupons.

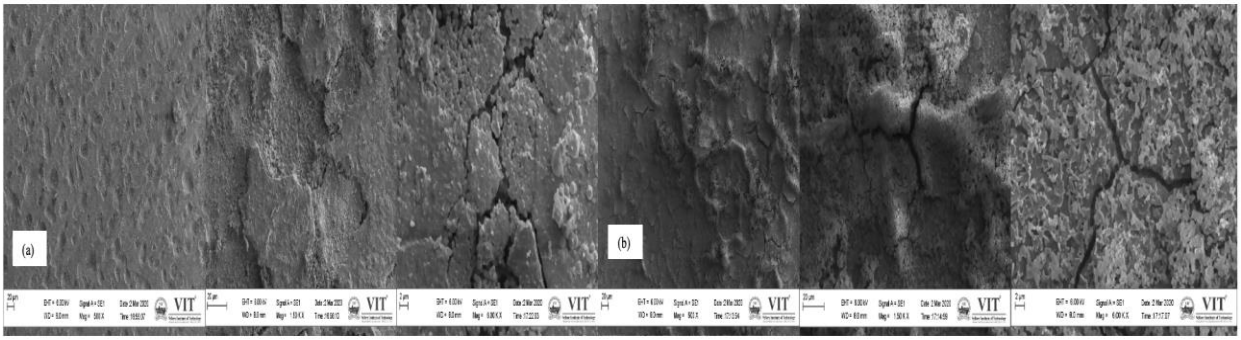

Figure S11. (a) Micrographs depicting formation of multiple pits on the metal surface post 336 h of bacterial trial taken at different magnification scales of 500x, 1000x, 1500x and 6000x. At 1500x and 6000x magnification, there is development of cracks with bacterial colonisation in between hence leading to successful corrosion of metal samples and (b) Micrographs depicting formation of multiple pits on the metal surface post 336 h of fungal trial taken at different magnification scales of 500x, 1000x, 1500x and 6000x. At 1500x and 6000x magnification, there is development of cracks with deposition of fungal mycelium in between hence leading to successful corrosion of metal samples